On relative permeability data uncertainty and CO_2 injectivity estimation for brine aquifers

Simon A. Mathias[a], Jon G. Gluyas[a], Gerardo J. González Martínez de Miguel[a,b], Steven L. Bryant[c], David Wilson[b]

[a]*Department of Earth Sciences, Durham University, Durham, UK*
[b]*ERC Equipoise Limited, London, UK*
[c]*Department of Petroleum and Geosystems Engineering, University of Texas at Austin, US*

Abstract

Performance assessment of possible CO_2 storage schemes is often investigated through numerical simulation of the CO_2 injection process. An important criterion of interest is the maximum sustainable injection rate. Relevant numerical models generally employ a multi-phase extension to Darcy's law, requiring data concerning the evolution of relative permeability for CO_2 and brine mixtures with increasing CO_2 saturation. Relative permeability data is acutely scarce for many geographical regions of concern and often cited as a major source of uncertainty. However, such data is expensive and time consuming to acquire. With a view to improving our understanding concerning the significance of relative permeability uncertainty on injectivity, this article presents a sensitivity analysis of sustainable CO_2 injection rate with respect to permeability, porosity and relative permeability. Based on available relative permeability data obtained from 25 sandstone and carbonate cores discussed in the literature, injectivity uncertainty associated with relative permeability is found to be as high as ±57% for open aquifers and low permeability closed aquifers (< 50 mD). However, for high permeability closed aquifers (> 100 mD), aquifer compressibility plays a more important role and the uncertainty due to relative permeability is found to reduce to ±6%.

Key words: Relative permeability, Geologic carbon sequestration, Pressure buildup

1. Introduction

There has been much effort focused on estimating volumetric CO_2 storage capacity in brine aquifers over large regional areas in many different countries. However, there is an increasing

understanding that such estimates are of limited value if not attached to some form of associated economic cost of utilization (Allinson et al., 2010). A major geologically dependent factor in this respect is the number of injection wells needed to utilize the storage capacity within a practical amount of time (Ehlig-Economides and Economides, 2010), which, in effect, is a measure of what many researchers refer to as injectivity.

Injectivity is dependent on many reservoir specific parameters, including permeability, porosity, formation thickness, areal extent, pressure, temperature, brine salinity and relative permeability (Mathias et al., 2011a). For regions with historic and contemporary oil and gas industries, estimates for these parameters are already available in national and corporate databases (e.g. Wilkinson et al., 2011). The exception to this are those parameters associated with CO_2-brine relative permeability, the reason being that (1) it has not been historically of interest to collect such information and (2) it is very expensive and time-consuming to obtain (Muller, 2011). Consequently, researchers are generally restricted to using data from the literature, often associated with different geological environments (e.g. Dria et al., 1993; Bennion and Bachu, 2008; Perrin and Benson, 2010; Pickup et al., 2011; Krevor et al., 2012).

In a recent study, Burton et al. (2009) found that uncertainty in relative permeability data can lead to a four-fold variation in injectivity. Specifically, Burton et al. (2009) estimated maximum sustainable injection rates using an approximate equation for predicting pressure build-up due to CO_2 injection into a brine aquifer (Burton et al., 2008). All parameters were held constant, including permeability and porosity, except for those associated with relative permeability. They repeated the simulations using relative permeability parameter sets from seven different core-flood experiments (reported previously by Bennion and Bachu, 2008). However, the nature of the simplifying assumptions used by Burton et al. (2009) may have overemphasized this point. Their approximate solution assumes fixed pressure boundaries at both the injection well face and the far-field boundary and that both the brine and CO_2 are incompressible. Consequently, at the start of injection, the pressure profile corresponds to one that would be expected for steady state injection of brine (with the same constant injection pressure). As CO_2 is introduced, the CO_2 injection rate increases as a consequence of an increase in bulk mobility associated with the lower viscosity of CO_2 (as compared to brine). The main control on this change in mobility are the relative

permeability parameters.

If instead an initially uniform pressure distribution is considered, at the start of injection there is a spatial step change in pressure from the injection well to the boundary of the aquifer. With time, this pressure front moves out and becomes more attenuated. The migration of the pressure wave is controlled by the intrinsic permeability of the formation and the bulk compressibility of the reservoir fluid and formation. Such a scenario predicts CO_2 injection rate to be highest at the beginning of the simulation. With time, as the pressure gradients reduce, in contrast to the Burton et al. (2009) study, there will be a corresponding reduction in CO_2 injection rate (for the constant injection well pressure scenario). For this more realistic scenario, it can be imagined that intrinsic permeability and compressibility play will play a more important role on injectivity.

More recently, Mathias et al. (2011b) derived a semi-analytical solution for pressure buildup due to constant rate of CO_2 injection into a closed brine aquifer with an initially uniform pressure distribution. Their model extends work previously presented by Mathias et al. (2009) and Mathias et al. (2011a) by allowing for non-linear relative permeability and partial miscibility between the CO_2 and brine. In this study, following the idea of Burton et al. (2009), the role of relative permeability is studied by simulating CO_2 injection into formations of various permeabilities, porosities, radial extents of aquifer, reservoir conditions and brine salinities with each scenario repeated for 25 different relative permeability parameter sets for sandstone and carbonate formations currently available from the literature (Bennion and Bachu, 2008; Perrin and Benson, 2010; Krevor et al., 2012).

The structure of this article is as follows: Firstly, the relative permeability data sets selected from the literature are discussed. Relevant results from numerical simulation, using TOUGH2 (Pruess et al., 1999) with ECO2N (Pruess, 2005; Pruess and Spycher, 2007), of the CO_2 injection problem are presented. The accuracy of the aforementioned semi-analytical solution for non-linear relative permeabilities is verified by comparison with simulation output from the numerical simulator. Discussion is given with regards to parameterizing permeability reduction due to salt precipitation. Results from a sensitivity analysis, using the pressure buildup equation of Mathias et al. (2011b), are then presented and discussed.

2. Relative permeability data

Relative permeability characteristics are often represented in numerical and mathematical reservoir simulators by power laws of the form (e.g. Orr, 2007):

$$k_{ra} = k_{ra0}\left(\frac{1 - S_g - S_{ar}}{1 - S_{gc} - S_{ar}}\right)^m \tag{1}$$

$$k_{rg} = k_{rg0}\left(\frac{S_g - S_{gc}}{1 - S_{gc} - S_{ar}}\right)^n \tag{2}$$

where k_{ra} [-] and k_{rg} [-] are the relative permeabilities for the aqueous and CO_2 rich phases, respectively (hereafter, referred to, for convenience, as the aqueous and gas phase, respectively), S_g [-] is the gas phase volumetric saturation (i.e., the volumetric proportion of pore-space occupied by CO_2 rich phase), S_{ar} [-] is the residual aqueous phase saturation, S_{gc} [-] is the critical gas saturation, and k_{ra0} [-], k_{rg0} [-], m [-] and n [-] are the end-point relative permeabilities and power-law exponents for the aqueous and gas phases, respectively.

Bennion and Bachu (2008, 2010) present parameters for Eqs. (1) and (2) for a range of sandstone, carbonate and cap-rock formations from Alberta, Canada. These data were obtained from transient drainage and imbibition experiments for CO_2-brine mixtures at various reservoir conditions. Rather than deriving values of relative permeability for specific values of saturation, such as is often done with variations of the so-called JBN method (Johnson et al., 1959), Bennion and Bachu (2008, 2010) use a history matching technique similar to that described by Sigmund and McCaffery (1979). In this way, the relative permeability parameters for Eqs. (1) and (2) are derived directly from the pressure buildup and fluid recovery data measured during the experiments.

The various formations were studied at a range of different pressures, temperatures and salinities so as to better represent their associated in situ environments. Pressure, temperature and salinity mostly affect relative permeability through the interfacial tension (IFT) that develops between the brine and CO_2. High IFT tends to lead to greater non-linearity between relative permeability and fluid saturation (Bachu and Bennion, 2008). Permeability, porosity, IFT and relative permeability parameter values (for Eqs. (1) and (2)) are summarized for the Bennion and Bachu (2008, 2010) drainage experiments on sandstone and carbonate cores in Table 1. Note that Bennion and

Bachu (2008, 2010) assumed $k_{ra0} = 1$ and $S_{gc} = 0$ for all the drainage experiments.

Perrin and Benson (2010) obtained relative permeability data for a heterogenous sandstone core provided by the CO2CRC-Otway project and a more homogenous Berea sandstone core. For both cases, relative permeability data was obtained by performing a sequence of steady-state drainage experiments, under reservoir conditions, whereby initially brine saturated cores were injected with CO_2-brine mixtures of sequentially increasing CO_2 content. Volume averaged CO_2 saturations of the cores were measured using an X-ray CAT scanner. The final results took the form of a set of discrete relative permeability and CO_2 saturation data for each of the steady-state saturations achieved.

Krevor et al. (2012) used a similar method to Perrin and Benson (2010) and obtained relative permeability data for four more sandstone cores including Berea Sandstone, Paaratte Formation (also from Otway, Australia), Mt. Simon Formation (Illinois, US) and Tscaloosa Formation (from the Cranfield CO_2 injection site, Mississippi, US).

To aid comparison of the Perrin and Benson (2010) and Krevor et al. (2012) data with that from Bennion and Bachu (2008, 2010), we have obtained corresponding parameters for Eqs. (1) and (2) by least-squares fitting to the data given in Figs. 9 and 13 of Perrin and Benson (2010) and Fig. 13 of Krevor et al. (2012). These are additionally summarized alongside associated values of permeability, porosity and IFT in Table 1. To be consistent with Bennion and Bachu (2008, 2010), we uniformly assumed $k_{ra0} = 1$ and $S_{gc} = 0$ (this was found to have very little impact on goodness of fit with the data). Note that Krevor et al. (2012) provided parameter fits for Brooks-Corey relations, which are different to the expressions given in Eqs. (1) and (2).

The relative permeability curves for all 25 parameter sets are plotted in Fig. 1. The sandstones are shown in Figs. 1a and b whilst the carbonates are shown in Figs. 1c and d. There is a very wide range of different responses. There are no obvious differences between the sandstone and carbonate formations. Even for repeat runs on the same formations, there are wide variations in both non-linearity and end-point relative permeability (e.g. Berea #1 and #2). There is also little difference between results obtained using steady-state and transient experimental methods (compare Figs. 1a and b). Note that both methods yielded low (e.g. Tuscaloosa and Ellerslie) and high (e.g. Otway and Cardium #1) end-point relative permeabilities. See Muller (2011) for further

discussion on the differences between these two methods.

3. Simulation of CO_2 injection in brine aquifers

It is clear from Table 1 and Fig. 1 that a wide range of relative permeability characteristics can be expected from reservoir rocks of interest in the future. As stated earlier, to better understand the importance of this uncertainty on CO_2 injectivity, here we consider the semi-analytical pressure buildup equation recently presented by Mathias et al. (2011b).

The equation predicts pressure buildup as a consequence of a constant mass injection rate of CO_2 into a closed or open brine aquifer. Building heavily on the work of Nordbotten et al. (2005), Orr (2007), Zeidouni et al. (2009) and Mathias et al. (2009, 2011a), derivation of the equation involves invoking of a number of simplifying assumptions including:

1. Vertical pressure equilibrium;
2. Negligible capillary pressure;
3. Constant fluid properties;
4. Homogenous, isotropic and cylindrical aquifer formation;
5. Constant mass injection rate through a centrally located fully completed vertical well;
6. Formation is confined above and below (lateral confinement is optional).

From comparison with isothermal simulations from TOUGH2, Mathias et al. (2009, 2011a) found the first three assumptions not to be important for pressure buildup providing an appropriate reference pressure is used to estimate the constant CO_2 fluid properties. However, all the simulations studied assumed linear relative permeability functions. Therefore, to further test the validity of the semi-analytical solution, additional TOUGH2 (Pruess et al., 1999) simulations, with the equation of state module, ECO2N (Pruess, 2005; Pruess and Spycher, 2007), were performed with increasingly non-linear relative permeability.

The ECO2N module provides a number of different relative permeability functions that can be chosen. However, to be consistent with the CO_2 and brine relative permeability data sets given in Table 1, we implemented the equations given in Eqs. (1) and (2). As within the studies of Mathias

et al. (2011a), gas saturation was assumed to be related to capillary pressure, P_c [$\mathrm{ML^{-1}T^{-2}}$], via the van Genuchten (1980) function

$$\frac{1 - S_g - S_{ar}}{1 - S_{gc} - S_{ar}} = \left(1 + \left|\frac{P_c}{P_{c0}}\right|^{n_v}\right)^{-m_v}, \quad n_v = \frac{1}{1 - m_v} \tag{3}$$

where m_v [-] is another empirical parameter. The parameters P_{c0} [$\mathrm{ML^{-1}T^{-2}}$] and m_v [-] are empirical parameters taken to be the same values as those used in the saline aquifer studies of Zhou et al. (2008).

To study the effect of non-linearity, a scenario similar to Scenario c) presented by Mathias et al. (2011a) was simulated with different values of m with $m = n$ (recall that Mathias et al. (2011a) only studied the linear relative permeability case when $m = n = 1$). The full set of parameters used are listed in Table 2.

All the simulations assumed vertical pressure equilibrium and were setup as one-dimensional axially symmetric problems. See Mathias et al. (2011a,b) for further discussion concerning vertical pressure equilibrium in this context. Following Mathias et al. (2009), the location of the discretized points in space were distributed logarithmically to ensure higher resolution at the injection well.

Fig. 2a compares well pressures from the semi-analytical solution (the solid lines) with those from TOUGH2 (the circular markers). The results from the semi-analytical solution were obtained by assuming a pressure of 18 MPa for the constant fluid properties. Fluid properties for CO_2 and brine mixtures were estimated using MATLAB implementations of equations presented by Batzle and Wang (1992), Spycher et al. (2003); Spycher and Pruess (2005) and Fenghour et al. (1998).

Both the semi-analytical solution and TOUGH2 predict pressure to rise monotonically with time. Increasing the non-linearity of the relative permeability functions (i.e., increasing m) leads to an almost constant increase in pressure. The plots confirm that the close correspondence between well pressures from the semi-analytical solution and TOUGH2 is not diminished with increasingly non-linear relative permeability functions.

At this point it is also interesting to re-examine Burton et al. (2008)'s approximation. Burton et al. (2008, 2009) avoid numerical integration by assuming uniform relative permeabilities within the two-phase region based on the arithmetic mean of the CO_2 saturation at the trailing and leading

shock fronts. In this way, it is assumed that (referring explicitly to Eq. (58) of Mathias et al. (2011b))

$$F_2(z) = \frac{1}{\mu_g}\int_z^{z_L}\left(\frac{k_{ra}}{\mu_a}+\frac{k_{rg}}{\mu_g}\right)^{-1}\frac{1}{z}dz \approx \frac{1}{\mu_g}\left(\frac{k_{ra}}{\mu_a}+\frac{k_{rg}}{\mu_g}\right)^{-1}_{S_g=(S_{gT}+S_{gL})/2}\ln\left(\frac{z_L}{z}\right) \tag{4}$$

where z is a similarity transform found from

$$z = \frac{\pi\phi\rho_c H r^2}{M_0 t} \tag{5}$$

and μ_a [$\mathrm{ML^{-1}T^{-1}}$] and μ_g [$\mathrm{ML^{-1}T^{-1}}$] are the dynamic viscosities of the aqueous and gas phase, respectively, z_L is the value of z at the front of the CO_2 plume (i.e., the location of the leading shock), ϕ [-] is porosity, ρ_c [$\mathrm{ML^{-3}}$] is the density of pure CO_2, H [L] is formation thickness, r [L] is radial distance from the well, M_0 [$\mathrm{MT^{-1}}$] is mass injection rate of CO_2 and t [T] is time after start of injection.

However, it is still necessary to find the locations of the shock fronts by iterative solution of Eq. (30) of Mathias et al. (2011b). Results for well pressures using Burton's approximation are plotted as dashed lines in Fig. 2a alongside those from the TOUGH2 simulation and the semi-analytical solution. Well pressures predicted using Burton's approximation tend to overestimate those from the semi-analytical solution and TOUGH2. However, this error appears to decrease with increasingly non-linear relative permeability functions.

Profile plots of gas saturation and pressure against radial distance for various times, obtained using TOUGH2 (circular markers), the semi-analytical solution (solid lines) and Burton's approximation (dashed lines), are plotted for the $m = 3$ case in Figs. 2b and c, respectively. Again, the close correspondence between TOUGH2 and the semi-analytical solution is undiminished. Note that Burton's approximation gives rise to a linear-log pressure profile in the two-phase region, which closely follows that from TOUGH2 and the numerically integrated semi-analytical solution. Clearly Burton's method is a useful alternative to numerically evaluating the integral in Eq. (4). However, if one is in a position to iteratively solve Eq. (30) of Mathias et al. (2011b), accurate numerical integration of Eq. (58) of Mathias et al. (2011b) is quite a trivial extra step.

Iterative solution of Eq. (30) of Mathias et al. (2011b), for the shock front locations, was

achieved using MATLAB's optimization routine, FMINSEARCH. Numerical integration of Eq. (58) of Mathias et al. (2011b) was achieved using the trapezoidal method (via MATLAB's TRAPZ function) with z values obtained from a corresponding vector of 200 equally spaced values of S_g between S_{gL} and S_{gT}. Results shown for when $m = n = 1$ were obtained from the closed-form equations for this special case, also given in Mathias et al. (2011b). It is demonstrated here that the numerically integrated semi-analytical solution of Mathias et al. (2011b) is an accurate alternative to TOUGH2 ECO2N for the non-linear relative permeability simulation scenarios considered. In the following sections, the semi-analytical solution is used to explore the role of uncertainty concerning relative permeability on pressure-buildup by sensitivity analysis.

Recall that the well pressures plotted in Fig. 2a are all monotonically increasing with time. Numerically simulated constant rate CO_2 injections are often reported to lead to non-monotonic well pressure behavior in the form of an early-time pressure spike (e.g. Zhou et al., 2008; Chadwick et al., 2009; Okwen et al., 2011). Indeed, we have also observed a spike in pressure at early times from simulations undertaken using TOUGH2, ECLIPSE-100 and CMG-GEM. However, on increasing the grid resolution around well it is found that the pressure spike decreases in duration. Furthermore, once sufficient grid resolution is realized, the pressure spike ultimately vanishes, in accordance with the monotonic results predicted by the semi-analytical solution. Similar results are also reported by Pickup et al. (2012). The grid used to obtain the results given in Fig. 2 employed 451 logarithmically spaced points with the first element (next to the well) being of 1 mm length.

4. Permeability reduction due to salt precipitation

In the previous section, the permeability reduction factor due to salt precipitation, k_{rs} [-], was set to one throughout (i.e., it was assumed that salt precipitation led to no permeability reduction). To incorporate the effect of salt precipitation on permeability reduction in our subsequent analysis, we have employed the experimental data obtained by Bacci et al. (2011) for a St Bees sandstone core (Fig. 3).

Previous researchers have used the Verma and Pruess (1989) model for this purpose, commonly with the so-called Γ and ϕ_r parameters somewhat arbitrarily set to 0.8 (after Pruess et al., 1999).

Through least-squares fitting we found $\Gamma = \phi_r = 0.57$ leads to a good fit to the experimental data (see Fig. 3). However, a better fit is obtained by linear regression of the power law

$$k_{rs} = \frac{k}{k_0} = \left(\frac{\phi}{\phi_0}\right)^{\eta} \tag{6}$$

where k [L^2], k_0 [L^2], ϕ [-], ϕ_0 [-] are current permeability, initial permeability, current porosity and initial porosity, respectively and η [-] is an empirical exponent. Linear regression yields an η value of 5.74 (see Fig. 3). Note that $\phi/\phi_0 = 1 - S_s$ where S_s [-] is the volumetric saturation of participated salt (see Eq. (38) of Mathias et al., 2011b). For the remainder of the analysis, k_{rs} is calculated from Eq. (6) with $\eta = 5.74$.

Kim et al. (2012) usefully distinguish between non-localized and localized salt precipitation. Non-localized salt precipitation is characterized by uniform salt precipitation within the dry-out zone, which largely comes about due to vaporization of residually trapped brine. Localized salt precipitation is characterized by an abnormally high level of salt precipitation at the dry-out front, where strong capillary forces cause displaced brine to re-imbibe back towards the well.

Recall that the semi-analytical solution, discussed in the previous section, ignores capillary forces. Consequently, this localized salt precipitation is unaccounted for in the analysis described in this paper. However, capillary driven back flow is likely to reduce with increasing injection rate. Interestingly, comparing results from models which ignored and included capillary pressure (and in turn, counter current imbibition), Pruess and Muller (2009) found that inclusion of capillary pressure effects is unlikely to increase salt precipitation by more than a factor of order 1.1. Furthermore, notable changes in the shape of the dry-out zone, as a result of counter current imbibition, were only observed for the exceptionally small injection rate of 0.025 kg/s/m per unit length of fully completed vertically orientated well screen (see their Fig. 7). It is expected that accounting for localized salt precipitation would not lead to significant differences in conclusions to the analysis described in our article.

5. Dimensionless pressure buildup contribution due to relative permeability

Pressure buildup due to CO_2 injection in brine aquifers is dependent on many characteristics in addition to relative permeability, in particular, reservoir volume, porosity, permeability and injection duration. However, it is possible to separate out these effects by simple manipulation of the equations presented by Mathias et al. (2011b). Recall in Fig. 2a that increasing the relative permeability non-linearity led to a relatively constant increase in pressure. Inspection of Eq. (57) of Mathias et al. (2011b) reveals that for large time, almost all of the relative permeability characteristics within the pressure buildup equation takes the form of the following dimensionless constant, P_{rpD} [-], found from

$$P_{rpD} = \frac{1}{\mu_c}\left[\frac{\mu_c}{k_{rs}}\ln z_T + \mu_g q_{D2} F_2(z_T) - \mu_b q_{D3}\ln z_L\right] \tag{7}$$

where μ_c [$ML^{-1}T^{-1}$] and μ_b [$ML^{-1}T^{-1}$] are the dynamic viscosities of pure CO_2 and CO_2-free-brine, respectively, F_2 is found from the integral form of Eq. (4), z_T is the value of z at the edge of the dry-out zone (that develops around the well due to brine vaporization) and q_{D2} [-] and q_{D3} [-] are dimensionless volumetric flow reductions due to brine vaporization and CO_2 dissolution, respectively. Note that z_T and z_L are both constants.

Calculation of all the terms given in Eq. (7) require additional auxiliary functions described in detail by Mathias et al. (2011b). But the important point to note is that, given an equation of state for the CO_2-brine mixture, $P_{rpD} = f(P_{\text{ref}}, T, \omega_{sb}, S_{ar}, S_{gc}, k_{ra0}, k_{rg0}, k_{rs}, m, n)$, where P_{ref} [$ML^{-1}T^{-2}$], T [θ], ω_{sb} [-] are the reference pressure, temperature and salt mass fraction in brine needed for calculation of the various relevant fluid properties. Therefore for a given set of reservoir conditions (P_{ref}, T, ω_{sb}), it is possible to assess the relative significance of the 25 relative permeability parameter sets given in Table 1 by the constant values provided by Eq. (7).

Values of P_{rpD} were calculated for the 25 parameter set, assuming $P_{\text{ref}} = 15$ MPa, $T = 40$ ^oC and $\omega_{sb} = 0.15$. Each value is plotted against k_{rg0}, S_{ar}, m and n in Figure 4. It can be seen that there are a wide range of P_{rpD} values from close to zero up to 221. The largest P_{rpD} values correspond with the smaller k_{rg0} values. The smallest P_{rpD} values correspond with those values of brine exponent, m, closest to unity (i.e., approaching linear brine relative permeability). There is

also some tendency of P_{rpD} increasing with S_{ar}, presumably because larger values of S_{ar} tend to correspond with smaller values of k_{rg0}. There seems to be no obvious trend with the CO_2 exponent, n, and there is little difference between the response of the sandstone and carbonate cores. The largest P_{rpD} value is attributable to the Tuscaloosa formation. Although Tuscaloosa does not have the smallest k_{rg0}, it has moderate to large values for S_{ar}, m and n. The value of P_{rpD} is not strongly dependent on any single parameter, rather it is controlled by the combined parameter set as a whole.

Fig. 5 shows a plot of porosity against permeability for the 25 parameter sets. As is normally observed, larger porosities tend to lead to larger permeabilities. Bachu and Bennion (2008) observed a good correlation between permeability and k_{rg0}, although only after excluding one of 13 rock samples. Fig. 6 shows plots of k_{rg0}, S_{ar}, m, n and P_{rpD} against porosity, permeability and IFT for all 25 parameter sets. Again, there is no obvious difference between the sandstone and carbonate cores. Contrary to Bachu and Bennion (2008), Fig. 6f shows no link between k_{rg0} and permeability. There is an interesting pattern between m and ϕ in Fig. 6c, but only for $\phi > 15\%$. But more importantly, for the 25 parameter sets studied, there is no apparent link between P_{rpD} and lithology, permeability, porosity and/or IFT (see Figs. 6 e, j and o).

6. Injectivity sensitivity analysis

From Figs. 6e, j and o it can be concluded that: (1) the 25 relative permeability parameter sets (RPPS) given in Table 1 are likely to lead to a wide range of injectivities; (2) there is no apparent link between lithology, porosity, permeability and/or IFT with relative permeability. It is therefore interesting to propagate the uncertainty associated with the 25 RRPS (i.e., k_{rg0}, S_{ar}, m, n) through to injectivity for a range of practical dimensional scenarios of interest.

Consider the base case described in Table 3. Figs. 7a to d show pressure responses predicted by the semi-analytical solution using the 25 RPPS. Maximum sustainable injection rates for each RPPS were obtained by iteration such that the well pressure equals P_{max} after 30 years. The individual injection rates are detailed in the legends given in Figs. 7a to d. Note that this analysis ignores the porosity and permeability data given in Table 3 and uses only the RPPS (i.e., k_{rg0}, S_{ar}, m, n).

Not surprisingly (given the discussion in the previous section), the Tuscaloosa Sandstone yields the lowest injection rate at 5.4 kg/s. The largest injection rate is achieved using the Slave Point Carbonate at 13.1 kg/s. Therefore, for the scenario depicted by the parameters given in Table 3, uncertainty concerning RPPS has led to a 2.4-fold variation in injection. Recall that Burton et al. (2009) observed a 4-fold variation in injectivity for their considered scenario. Limiting the study to the cores studied by Burton et al. (2009) (Wabamun #1, Basal Cambrian, Wabamun #2, Nisku #1, Viking #1, Ellerslie, Cooking Lake #1), the minimum and maximum injection rates are 9.4 kg/s and 12.1 kg/s from Ellerslie and Wabamun #1, respectively, leading to a 1.3-fold variation.

As discussed in the introduction, the analysis of Burton et al. (2009) ignores the compressibility of the aquifer. In this case, the amount of CO_2 that can be injected into the aquifer is dependent only on the RPPS and the permeability of the aquifer. For the compressible closed aquifer scenario, represented by the parameters in Table 3, compressibility plays an additional role on injectivity and hence the importance of uncertainty in RPPS is reduced.

Fig. 8a shows plots of maximum sustainable injection rate for each of the 25 RPPS for the base case described in Table 3 but for different reservoir permeabilities and porosities, as indicated by the x-axis and legend, respectively. For small permeabilities, results for the three porosities converge as injection capacity becomes permeability limited and independent of available pore-volume. For large permeabilities, injection capacity flattens off with permeability and there is a greater variation with porosity. This can be explained as follows: For small injection rates (associated with small permeabilities), the associated pressure wave does not have time reach the outer boundary of the aquifer, during the 30 year period studied. Hence for small injection rates, the reservoir units are insensitive to the total available pore-volume and are acting as would be expected for infinite units (consider Eq. (59) of Mathias et al. (2011b)). For larger injection rates (associated with large permeabilities), the associated pressure wave reaches the outer boundary of the aquifer during the 30 year period. In this case, the reservoir units become less sensitive to permeability and more dependent on the bulk aquifer compressibility.

For the range of permeabilities and porosities studied, injectivity variation associated with uncertainty in relative permeability is a fraction of that for permeability and porosity. Note that the minimum and maximum injection rates are due to the Tuscaloosa Sandstone and Slave Point

Carbonate, respectively.

The black solid and dashed lines in Fig. 8a are the mean and mean ± two standard deviations (which for normally distributed data corresponds to the 50, 97.7 and 2.3 percentiles, respectively) of injection rates for 25 RPPS. Interestingly, it is the Ellerslie sandstone (highlighted in yellow) that most closely follows the mean response. Furthermore, if one wanted to use linear permeability functions (i.e., $m = n = 1$, so as to benefit from the closed-form expressions for the locations of the two shock fronts given by Mathias et al. (2011b)) it is found that $k_{rg0} = 0.1$ and $S_{ar} = 0.2$ gives a good approximation to the mean response (the white circular markers).

Fig. 8b shows an equivalent plot of percentage variation in injection rate (PVIR) associated with the 25 RPPS, obtained by dividing two standard deviations by the mean and multiplying by 100. Independent of porosity, the PVIR = 47% for low permeabilities ($k \ll 100$ mD). However, with increasing permeability, the PVIR decreases to between 7% and 13%.

Fig. 9 shows plots of mean and ± two standard deviations for the base case scenario but with a), b), c) and d) looking at sensitivity to aquifer size, injection duration, reservoir conditions and formation water salinity, respectively. Maximum sustainable injection rate is seen to increase with increasing aquifer size, decreasing injection duration, increasing aquifer depth (assuming hydrostatic conditions and a 40^oC/km geothermal gradient) and reducing brine salinity. Maximum sustainable mass injection rate increases with depth mainly because brine vaporization increases with increasing temperature (see Fig. 2 of Spycher and Pruess, 2005). Reducing salinity reduces the amount of permeability loss due to salt precipitation, increases the amount of CO_2 that dissolves into the brine and increases the amount of water that vaporizes into the CO_2 rich phase, all of which improve injectivity (see Fig. 2 of Spycher and Pruess, 2005). See Mathias et al. (2011b) for a detailed discussion concerning the role of partial miscibility on pressure buildup in this context.

Similar to Fig. 8b, Fig. 10 shows plots of PVIR for the scenarios reported in Fig. 9. As in Fig. 8b, Figs. 10a and b show PVIR declining with increasing permeability from a maximum value of 47%. Furthermore, it is shown that for the small aquifers ($r_E = 5$ km), a minimum PVIR of 6% is reached for permeabilities greater than 100 mD.

Fig. 10c shows that for, low permeabilities, there is an increase in PVIR from 47% to 57%

with increasing depth (assuming hydrostatic conditions and a 40^o C/km geothermal gradient). This is largely due to the increase in brine vaporization that occurs with increasing temperature. Fig. 10d shows that for, low permeabilities, there is an increase in PVIR from 44% to 55% with decreasing salinity. Note that PVIR for the base case but with no permeability reduction due to salt precipitation are also shown as green circular markers. It can be seen that permeability reduction has very little effect on PVIR. The increased PVIR with decreasing salinity is again more to do with changes in brine vaporization.

Interestingly, it can be seen that the results presented in Fig. 8b, Fig. 10b and c would collapse on to a single curve with the correct x-axis translation. Consideration of the inequality ($z_E < 0.5615/\alpha$) in Eq. (59) of Mathias et al. (2011b), beyond which the aquifer behaves as a closed aquifer (also see Mathias et al., 2011a), reveals that an appropriate x-axis variable for the PVIR plots is the dimensionless time

$$t_D = \frac{2.246kt}{\mu_b \phi (c_r + c_b) r_E^2} \tag{8}$$

where k [L^2] is permeability, c_r [$M^{-1}LT^2$] and c_b [$M^{-1}LT^2$] are the rock and brine compressibility, respectively, and r_E [L] is the radial extent of the aquifer.

Fig. 11 shows plots of PVIR against the dimensionless time given in Eq. (8) using the data previously presented in Figs. 8b, 10a and 10b. Indeed all the data collapses onto a single curve with PVIR declining from 47% to 6% with increasing t_D. Note, that the decline starts when $t_D = 1$, which is when enough time has passed for the pressure wave, associated with the CO_2 injection, to reach the outer boundary of the aquifer (see Mathias et al., 2011a). Once the pressure wave reaches the outer boundary, pressure buildup proceeds as if in a closed tank. Consequently, compressibility plays a more important role on injectivity and the importance of relative permeability uncertainty reduces.

7. Summary and conclusions

The objective of this study was to explore the possible impact of uncertainty associated with relative permeability parameters on estimation of injectivity for potential CO_2 storage sites in brine

aquifer formations. Pressure buildup due to CO_2 injection into a closed structure was estimated using the semi-analytical solution recently presented by Mathias et al. (2011b). Injectivity was assessed by studying the maximum constant CO_2 injection rate that can be sustained for 30 years without exceeding an injection pressure of 15 MPa, assuming an initial reservoir pressure of 10 MPa. A sensitivity analysis on injectivity was undertaken by estimating maximum constant CO_2 injection rate for a wide range of permeability, porosity, aquifer extent and reservoir conditions assuming the relative permeability parameter sets (RPPS) (i.e., k_{rg0}, S_{ar}, m, n) for each of 12 sandstone cores and 13 carbonate cores obtained from the literature in Table 1 (after Bennion and Bachu, 2008, 2010; Perrin and Benson, 2010; Krevor et al., 2012).

Permeability reduction due to salt precipitation was incorporated using a new power law fit to the experimental data recently obtained by Bacci et al. (2011) for a St Bees Sandstone rock core (see Fig. 3).

Inspection of the large time component of the semi-analytical solution, previously presented by Mathias et al. (2011b), revealed that the effects of relative permeability can be expressed as a dimensionless constant, P_{rpD}, dependent only on the RPPS and, given an appropriate equation of state, pressure, temperature, brine salinity and permeability reduction due to salt precipitation (recall Eq. (7)). Plots of P_{rpD} against the individual relative permeability parameters (Fig. 4) confirms that although, low end-point relative permeability (k_{rg0}) often leads to low injectivity and a brine exponent (m) close to 1 (i.e. close to linear) often leads to high injectivity, the P_{rpD} is a composite response linked to the combined effects of all four individual relative permeability parameters. Furthermore, plots of P_{rpD} for each of the 25 RPPSs against their corresponding original porosity, permeability and interfacial tensions (IFT) (Figs. 6e, j and o) reveals no apparent link between relative permeability with porosity, permeability, IFT and/or lithology.

In the subsequent wider sensitivity looking at RPPS uncertainty in conjunction with other reservoir parameters it was found that variation of injectivity associated with relative permeability parameters was a fraction of that expected due to commonly identified uncertainties associated with permeability and porosity. Nevertheless, the percentage variation in maximum sustainable injection rate (PVIR) associated with the 25 RPPs was as high as ±60% for low permeability aquifers (< 50 mD) or high permeability open aquifers. However, PVIR reduced to ±6% for high

permeability closed aquifers (> 100 mD) (see Figs. 8 and 10).

Reinspection of the equations presented by Mathias et al. (2011b) led to the realization that PVIR from all the different sensitivity analysis (assuming $P_0 = 10$ MPa, $T = 40^o$C, $w_{sb} = 0.15$) collapsed on to a single curve when the dimensionless time, t_D, given in Eq. (8) is used as the x-axis (see Fig. 11). It was then noticed that for $t_D < 1$, PVIR = 47% and for $t_D > 1$, PVIR gradually declined to 6%. Interestingly, $t_D > 1$ indicates that injection duration has proceeded for sufficiently long such as to allow the pressure wave (associated with injection commencement) to reach the outer boundary of a closed aquifer.

It was found that the minimum and maximum injectivities were due to the RPPS of the Tuscaloosa Sandstone and Slave Point Carbonate, respectively. The mean response of the 25 RPPS was best by captured by the Ellerslie Sandstone. A linear relative permeability model with $k_{rg0} = 0.1$, $S_{ar} = 0.2$, $m = 1$ and $n = 1$ gives an alternative approximation to the mean response of the 25 RPPS. The latter should be of use to those wishing to benefit from the closed-form expressions for the locations of trailing and leading shocks given by Mathias et al. (2011b).

Looking back to Burton et al. (2009)'s finding that uncertainty due to RPPS gave rise to a 4-fold variation in injectivity prediction, the analysis presented in the current article improves on Burton et al. (2009)'s analysis by incorporating an additional 18 RRPSs and additionally accounting for aquifer compressibility. Interestingly, the upper PVIR of ±57%, for aquifers where insufficient time has passed for the pressure wave to hit the boundary of the aquifer, corresponds to a 3.7-fold variation. However, the lower limit of ±6% for high permeability closed aquifers corresponds to just a 1.1-fold variation in injectivity. Finally it can be concluded that whilst uncertainty in RRPS can have a substantial effect on injectivity estimation for open aquifers, for closed aquifers, the effects associated with formation compressibility plays a more important role.

8. Acknowledgements

We would like thank IJGGC reviewer, Andrew Cavanagh, for his many helpful and constructive comments. These led to a greatly improved final manuscript. This work was funded by the UK Knowledge Transfer Partnership (KTP) Scheme.

References

Allinson, W. G., Y. Cinar, P. R. Neal, J. Kaldi, L. Paterson (2010), CO_2 storage capacity - combining geology, engineering and economics, SPE Asia Pacific Oil & Gas Conference and Exbition, Brisbane, Australia SPE 133804.

Bacci, G., A. Korre, S. Durucan (2011), Experimental investigation into salt precipitation during CO_2 injection in saline aquifers, Energy Procedia, 4, 4450-4456, doi:10.1016/j.egypro.2011.02.399.

Bachu, S., D. B. Bennion (2008), Effects of in-situ conditions on relative permeability characteristics of CO_2-brine systems, Environ. Geol., 54, 1707–1722, doi:10.1007/s00254-007-0946-9.

Batzle, M., and Z. Wang (1992), Seismic properties of pore fluids, Geophysics, 57, 1396–1408.

Bennion D. B., S. Bachu (2008), Drainage and imbibition relative permeability relationships for supercritical CO_2/brine and H_2S/brine systems in intergranular sandstone, carbonate, shale, and annhydrite rocks, SPE Reservoir Eval. Eng., 11, 487–496.

Bennion D. B., S. Bachu (2010), Drainage and imbibition CO_2/brine relative permeability curves at reservoir conditions for carbonate formations, SPE Annual Technical Conference and Exhibition, Florence, Italy, SPE 134028.

Burton, M., N. Kumar, and S. L. Bryant (2008), Time-dependent injectivity during CO_2 storage in aquifers, SPE/DOE Improved Oil Recovery Symposium, Tulsa, SPE 113937.

Burton, M., N. Kumar, and S. L. Bryant (2009), CO_2 injectivity into brine aquifers: why relative permeability matters as much as absolute permeability, Energy Procedia, 1, 3091–3098, doi:10.1016/j.egypro.2009.02.089.

Chadwick, R. A., D. J. Noy, and S. Holloway (2009) Flow processes and pressure evolution in aquifers during injection of supercritical CO_2 as a greenhouse gas mitigation measure, Pet. Geosci., 15, 59–73, doi:10.1144/1354-079309-793.

Dria, D. E., G. A. Pope, and K. Sepehrnoori (1993) Three-Phase Gas/Oil/Brine Relative Permeabilities Measured Under CO2 Flooding Conditions, SPE Reservoir Eng., 18, 143–150, doi:10.2118/20184-PA.

Ehlig-Economides, C. A., and M. J. Economides (2010) Sequestering carbon dioxide in a closed underground volume, J. Pet. Sci. Eng., 70, 123–130, doi:10.1016/j.petrol.2009.11.002.

Fenghour, A., W. A. Wakeham, and V. Vesovic (1998), The viscosity of carbon dioxide, J. Phys. Chem. Ref. Data, 27, 31–44.

Georgiadis, A., G. Maitland, J. P. M. Trussler, A. Bismarck (2010), Interfacial tension measurements of the (H_2O + CO_2) system at elevated pressures and temperatures, J. Chem. Eng. Data, 55, 4168–4175, doi:10.1021/je100198g.

Johnson, E. F., D. P. Bossler, V. O. Naumann (1959), Calculation of relative permeability from displace experiments, Trans. AIME 216, 370–372.

Kim, K. Y., W. S. Han, J. Oh, T. Kim, J.-C. Kim (2012),Characteristics of salt-precipitation and the associated pressure build-up during CO_2 storage in saline aquifers, Transp. Porous Med. 92, 397–418, doi:10.1007/s11242-011-9909-4.

Krevor, S. C. M., R. Pini, L. Zuo, S. M. Benson (2012), Relative permeability and trapping of CO_2 and water in

493 sandstone rocks at reservoir conditions, Water Resour. Res. 48, W02532, doi:10.1029/2011WR010859.
494 Mathias S. A., P. E. Hardisty, M. R. Trudell, and R. W. Zimmerman (2009), Approximate solutions for pressure
495 buildup during CO_2 injection in brine aquifers, Transp. Porous Media, 79, 265–284, doi:10.1007/s11242-008-
496 9316-7.
497 Mathias S. A., G. J. Gonzalez Martinez de Miguel, K. E. Thatcher, and R. W. Zimmerman (2011a), Pressure buildup
498 during CO_2 injection into a closed brine aquifer, Transp. Porous Media, In Press, doi:10.1007/s11242-011-9776-z.
499 Mathias S. A., J. G. Gluyas, G. J. Gonzalez Martinez de Miguel, S. A. Hosseini (2011b), Role of partial miscibility
500 on pressure buildup due to injection of CO_2 into closed and open brine aquifers, Water Resour. Res. 47, W12525,
501 doi:10.1029/2011WR011051.
502 Muller, N. (2011), Supercritical CO_2-brine relative permeability experiments in reservoir rocksliterature review and
503 recommendations, Transp. Porous Media, 87, 367–383, doi:10.1007/s11242-010-9689-2.
504 Nordbotten, J. M., M. A. Celia and S. Bachu (2005), Injection and storage of CO_2 in deep saline aquifers: analytic
505 solution for CO_2 plume evolution during injection, Transp. Porous Media, 58, 339–360, doi:10.1007/s11242-004-
506 0670-9.
507 Okwen, R. T., M. T. Stewart, J. A. Cunningham (2011), Temporal variations in near-wellbore pressures during CO2
508 injection in saline aquifers, Int. J. Greenhouse Gas Control, In Press, doi:10.1016/j.ijggc.2011.07.011.
509 Orr Jr., F. M. (2007), Theory of Gas Injection Processes, Tie-Line Publications, Copenhagen, Denmark.
510 Perrin, J.-C., Benson, S.M. (2010), An experimental study on the influence of sub-core scale heterogeneities on CO_2
511 distribution in reservoir rocks, Transp. Porous Media, 82, 93–109, doi:10.1007/s11242-009-9426-x.
512 Pickup, G., Jin, M., Olden, P, Mackay, E., Sohrabi, M. (2011), A sensitivty study on CO_2 storage in saline aquifers,
513 SPE EUROPEC/EAGE Annual Conference and Exhibition, Vienna, Austria SPE 143054.
514 Pickup, G., Jin, M., Mackay, E. J. (2012), Simulation of near-well pressure build-up in models of CO_2 injection,
515 ECMOR XIII 13th European Conference on the Mathematics of Oil Recovery, Biarritz, France, 10-13 September
516 2012.
517 Pruess, K., C. M. Oldenburg, and G. Moridis (1999), TOUGH2 users guide, version 2.0. Report LBNL-43134,
518 Lawrence Berkeley National Laboratory, Berkeley, CA, USA.
519 Pruess, K. (2005), ECO2N: A TOUGH2 fluid property module for mixtures of water, NaCl, and CO_2. Report LBNL-
520 57952, Lawrence Berkeley National Laboratory, Berkeley, CA, USA.
521 Pruess, K. and N. Spycher (2007), ECO2N - A fluid property module for the TOUGH2 code for studies of CO_2 storage
522 in saline aquifers, Energy Convers. Manage., 48, 1761–1767, doi:10.1016/j.enconman.2007.01.016.
523 Pruess, K. and N. Muller (2009), Formation dry-out from CO_2 injection into saline aquifers: 1. Effects of solids
524 precipitation and their mitigation, Water Resour. Res., 45, W03402, doi:10.1029/2008WR007101.
525 Sigmund, P. M., F. G. McCaffery (1979), An improved unsteady-state procedure for dertermining relative-
526 permeability characterstics of heterigenous porous media, SPE J. 19, 15–28, SPE-6720-PA.

Spycher, N., K. Pruess and J. Ennis–King (2003), CO_2-H_2O mixtures in the geological sequestration of CO_2. I. Assessment and Calculation of Mutual Solubilities from 12 to 100 ^{o}C and up to 600 bar, Geochim. Cosmochim. Acta, 67, 3015-3031, doi:10.1016/S0016-7037(03)00273-4.

Spycher, N. and K. Pruess (2005), CO_2-H_2O mixtures in the geological sequestration of CO_2. II. Partitioning in chloride brines at 12100 ^{o}C and up to 600 bar, Geochim. Cosmochim. Acta, 69, 3309-3320, doi:10.1016/j.gca.2005.01.015.

van Genuchten, M. Th. (1980), A closed form equation for predicting the hydraulic conductivity of unsaturated soils, Soil. Sci. Soc. Am. J., 44, 892–898.

Verma, A., K. Pruess (1989), Thermohydrological conditions and silica redistribution near high-level nuclear wastes emplaced in saturated geological formations, Water Resour. Res., 93, 1159–1173.

Wilkinson, M., R.S. Haszeldine, A. Hosa, R. J. Stewart, S. Holloway, M. Bentham, K. Smith, R. Swarbrick, S. Jenkins, J. Gluyas, E. Mackay, G. Smith, S. Daniels, M. Raistrick (2011), Defining simple and comprehensive assessment units for CO2 storage in saline formations beneath the UK North Sea and continental shelf. Energy Procedia, 4, 4865–4872. doi:10.1016/j.egypro.2011.02.454.

Zeidouni, M., M. Pooladi-Darvish, and D. Keith (2009), Analytical solution to evaluate salt precipitation during CO_2 injection in saline aquifers, Int. J. Greenhouse Gas Control, 3, 600–611, doi:10.1016/j.ijggc.2009.04.004.

Zhou, Q., Birkholzer, J., Tsang, C., Rutqvist, J., 2008. A method for quick assessment of CO_2 storage capacity in closed and semi-closed saline formations. Int. J. Greenhouse Gas Control 2 (4), 626–639.

Table 1: Porosity, permeability, IFT and relative permeability parameters (assuming Eqs. (1) and (2)) for the drainage experiments previously presented by Bennion and Bachu (2008, 2010), Perrin and Benson (2010) and Krevor et al. (2012). IFT values for the Bennion and Bachu (2010) results are as reported in Bennion and Bachu (2010). IFT values for the Bennion and Bachu (2008) were obtained from Bachu and Bennion (2008). IFT values for the Perrin and Benson (2010) and Krevor et al. (2012) results were interpolated from values obtained by Georgiadis et al. (2010). Note that for all cores, $k_{rw0} = 1$ and $S_{gc} = 0$.

Unit	Lithology	Source	Porosity (%)	Permeability (mD)	IFT (mN/m)	k_{rg0} (-)	S_{ar} (-)	m (-)	n (-)
Otway	sandstone	Perrin and Benson (2010)	18.2	45	30.0	0.6594	0.4370	2.5	6.5
Berea #1	sandstone	Perrin and Benson (2010)	20.3	430	30.0	0.0700	0.5890	2.5	1.3
Berea #2	sandstone	Krevor et al. (2012)	22.1	914	32.0	0.3948	0.4438	3.2	2.6
Paaratte	sandstone	Krevor et al. (2012)	28.3	1156	32.0	0.3284	0.3894	4.6	3.0
Mt. Simon	sandstone	Krevor et al. (2012)	24.4	7.5	32.0	0.4929	0.4371	6.0	1.6
Tuscaloosa	sandstone	Krevor et al. (2012)	23.6	220	32.0	0.0767	0.7030	4.7	3.2
Cardium #1	sandstone	Bennion and Bachu (2008)	15.3	0.356	19.8	0.5260	0.1970	1.3	1.7
Cardium #2	sandstone	Bennion and Bachu (2008)	16.1	21.17	19.8	0.1290	0.4250	1.2	1.3
Viking #1	sandstone	Bennion and Bachu (2008)	12.5	2.7	32.1	0.3319	0.5580	2.9	3.2
Viking #2	sandstone	Bennion and Bachu (2008)	19.5	21.72	32.1	0.2638	0.4230	1.7	2.8
Ellerslie	sandstone	Bennion and Bachu (2008)	12.6	0.376	32.5	0.1156	0.6590	2.1	2.2
Basal Cambrian	sandstone	Bennion and Bachu (2008)	11.7	0.081	27.0	0.5446	0.2940	1.8	5.0
Wabamun #1	carbonate	Bennion and Bachu (2010)	7.9	0.018	29.5	0.5289	0.5950	1.4	5.6
Wabamun #2	carbonate	Bennion and Bachu (2010)	14.8	66.98	29.5	0.1883	0.5690	1.4	2.1
Wabamun #3	carbonate	Bennion and Bachu (2010)	15.4	54.3	29.5	0.1015	0.8520	2.8	5.8
Nisku #1	carbonate	Bennion and Bachu (2010)	9.7	45.92	34.6	0.1768	0.3300	2.8	1.1
Nisku #2	carbonate	Bennion and Bachu (2010)	10.4	21.02	34.6	0.0999	0.4920	2.7	4.6
Nisku #3	carbonate	Bennion and Bachu (2010)	10.9	74.4	34.6	0.1078	0.3970	2.3	2.9
Grosmont	carbonate	Bennion and Bachu (2010)	11.8	153.9	29.5	0.1101	0.5200	1.7	5.2
Morinville Leduc	carbonate	Bennion and Bachu (2010)	11.6	371.9	33.1	0.0746	0.5300	1.8	3.7
Redwater Leduc	carbonate	Bennion and Bachu (2010)	16.8	353.6	35.1	0.0476	0.6650	1.6	4.8
Cooking Lake #1	carbonate	Bennion and Bachu (2010)	9.9	65.3	35.7	0.0685	0.4760	1.4	5.6
Cooking Lake #2	carbonate	Bennion and Bachu (2010)	16.7	4.87	35.7	0.0940	0.5963	1.8	5.4
Slave Point	carbonate	Bennion and Bachu (2010)	9.9	0.217	29.5	0.5037	0.5460	1.6	1.2
Winnipegosis	carbonate	Bennion and Bachu (2010)	14.8	3.09	45.3	0.6117	0.2108	2.4	4.5

Table 2: Parameters used for the TOUGH2 simulations.

Parameter	Symbol	Value
Injection rate,	M_0	= 15 kg/s
Well radius,	r_W	= 0.2 m
Radial extent,	r_E	= 20 km
Porosity,	ϕ	= 0.2
Rock compressibility,	c_r	= 4.5×10^{-10} Pa^{-1}
Initial pressure,	P_0	= 10 MPa
Temperature,	T	= 40 ^{o}C
Mass fraction of salt in brine,	ω_{sb}	= 0.15
Residual brine saturation,	S_{ar}	= 0.5
Critical gas saturation,	S_{gc}	= 0.0
End-point relative permeability for brine,	k_{ra0}	= 1.0
End-point relative permeability for CO_2,	k_{rg0}	= 0.3
Permeability reduction factor due to salt precipitation,	k_{rs}	= 1
van Genuchten parameter,	m_v	= 0.46
van Genuchten parameter,	P_{c0}	= 19600 Pa
Formation thickness,	H	= 30 m
Permeability,	k	= 100 mD

Table 3: Base case parameters used for injectivity sensitivity analysis.

Parameter	Symbol	Value
Well radius,	r_W	= 0.2 m
Radial extent,	r_E	= 20 km
Porosity,	ϕ	= 0.2
Rock compressibility,	c_r	= 4.5×10^{-10} Pa^{-1}
Initial pressure,	P_0	= 10 MPa
Temperature,	T	= 40 ^{o}C
Mass fraction of salt in brine,	ω_{sb}	= 0.15
Critical gas saturation,	S_{gc}	= 0.0
End-point relative permeability for brine,	k_{ra0}	= 1.0
Permeability reduction factor due to salt precipitation,	k_{rs}	= $(1 - S_s)^{5.74}$
Formation thickness,	H	= 30 m
Permeability,	k	= 100 mD
Injection duration,	t	= 30 years
Maximum pressure,	P_{max}	= P_0 + 5 MPa
Reference pressure for fluid properties,	P_{ref}	= P_{max}

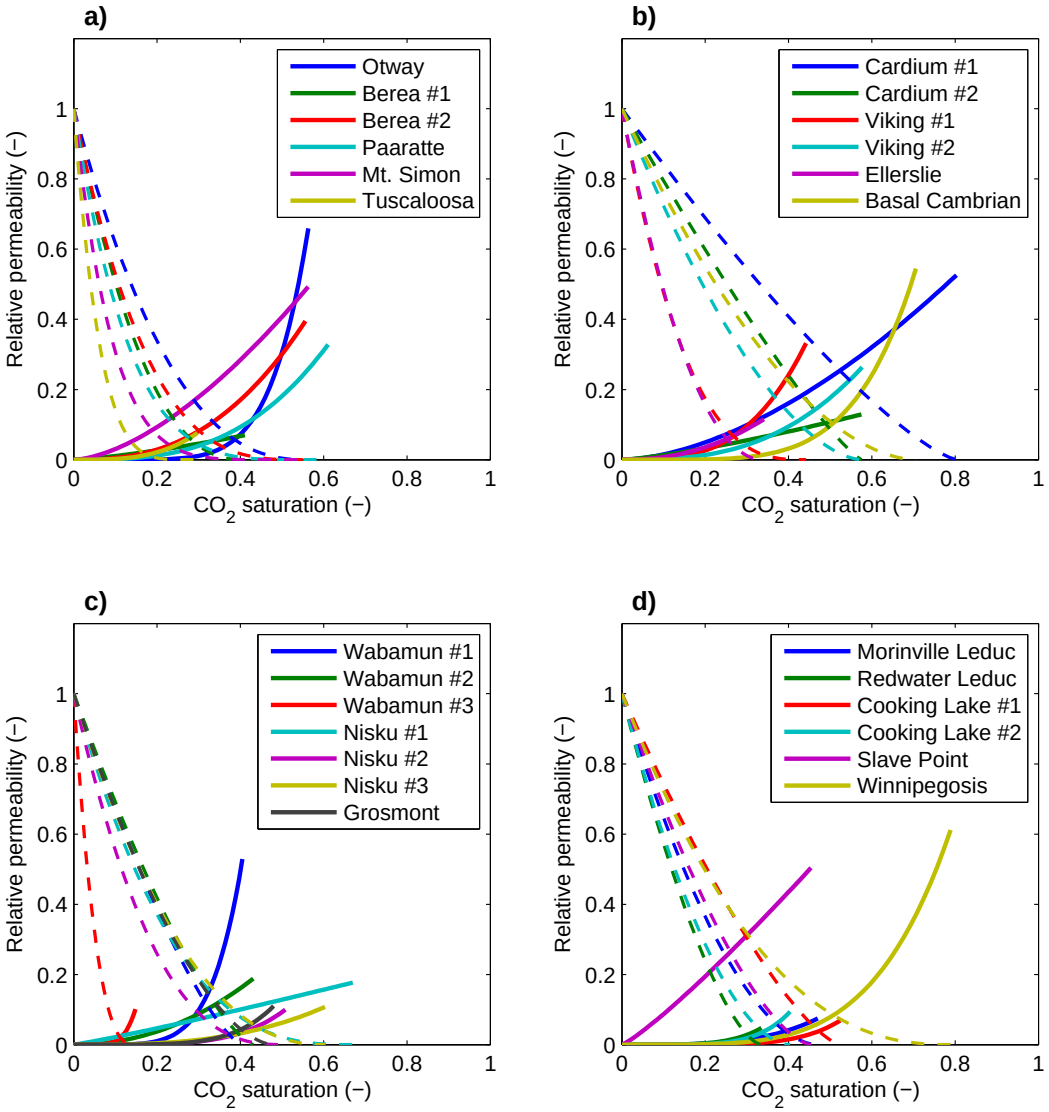

Figure 1: Relative permeability curves constructed using the power law functions in Eqs. (1) and (2) in conjunction with the parameters given in Table 1. Relative permeability for brine and CO_2 are shown as dashed and solid lines, respectively. a) Sandstone cores from Perrin and Benson (2010) and Krevor et al. (2012). b) Sandstone cores from Bennion and Bachu (2008). c) and d) Carbonate cores from Bennion and Bachu (2010).

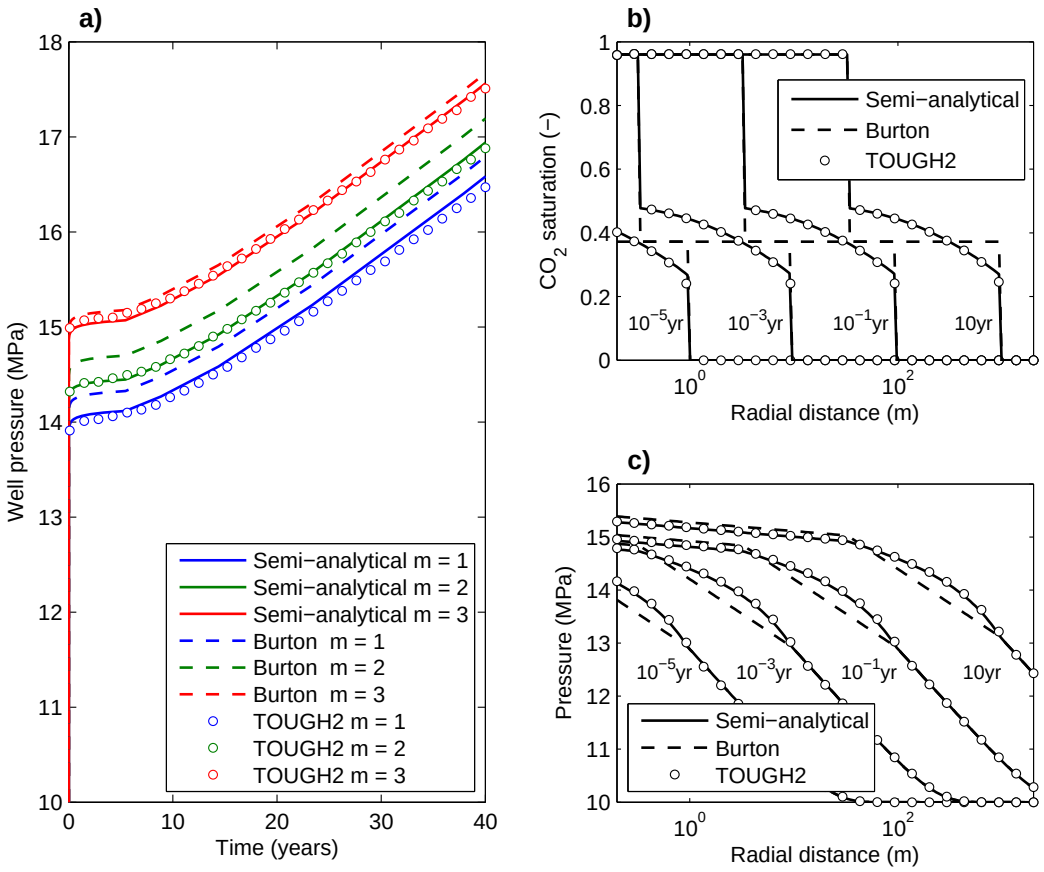

Figure 2: Comparison of the semi-analytical solution (solid lines), the semi-analytical solution with Burton et al. (2008)'s approximation (dashed lines) and TOUGH2 (circular markers). Note that all the simulations presented in this figure assumed n was equal to m. See Table 2 for other parameter values. a) Well pressures with m as indicated. b) CO_2 saturation with $m = 3$ and for times as indicated. c) Reservoir pressures with $m = 3$ and for times as indicated.

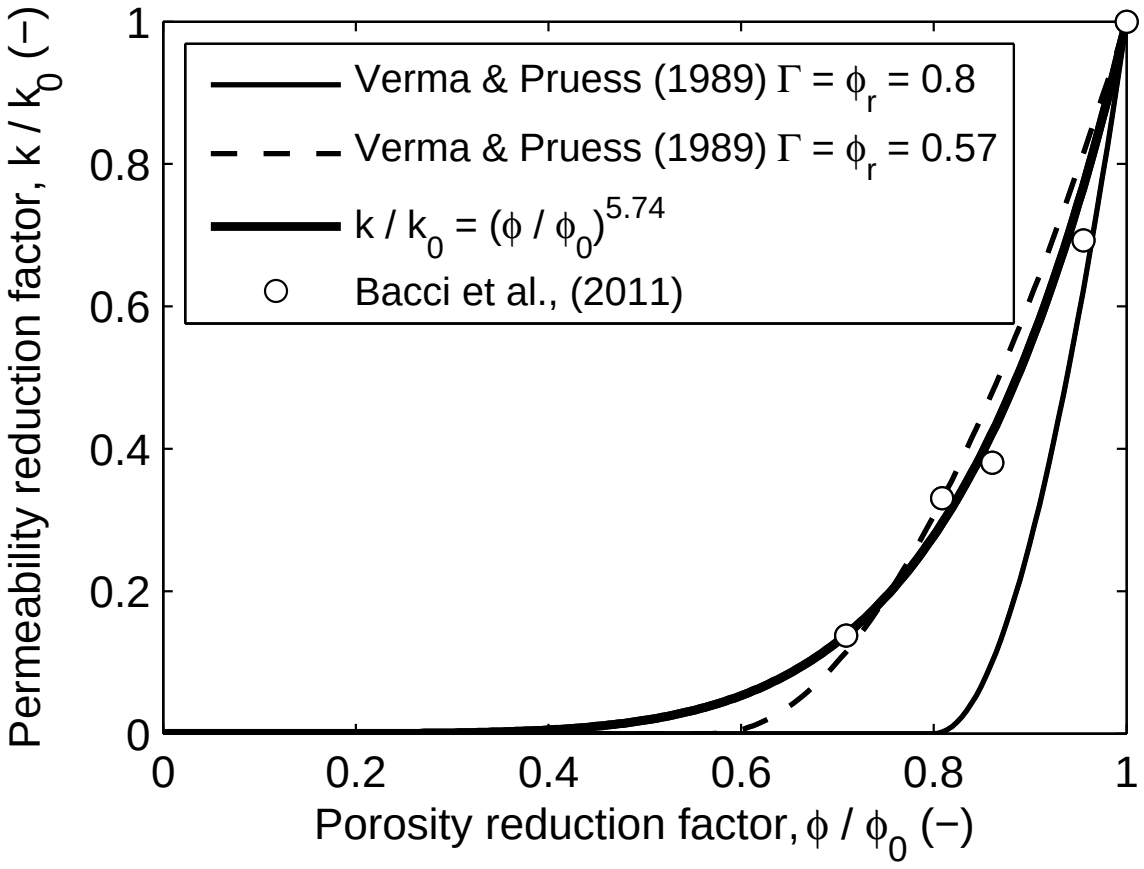

Figure 3: Plot of permeability reduction factor against porosity reduction factor due to salt precipitation. The Verma and Pruess (1989) model is shown with $\Gamma = \phi_r = 0.8$ and $\Gamma = \phi_r = 0.57$. The latter parameter value was obtained by fitting to the experimental data of Bacci et al. (2011), obtained from CO_2 flooding of a St Bees sandstone core. The empirical power law was obtained by linear regression with the experimental data.

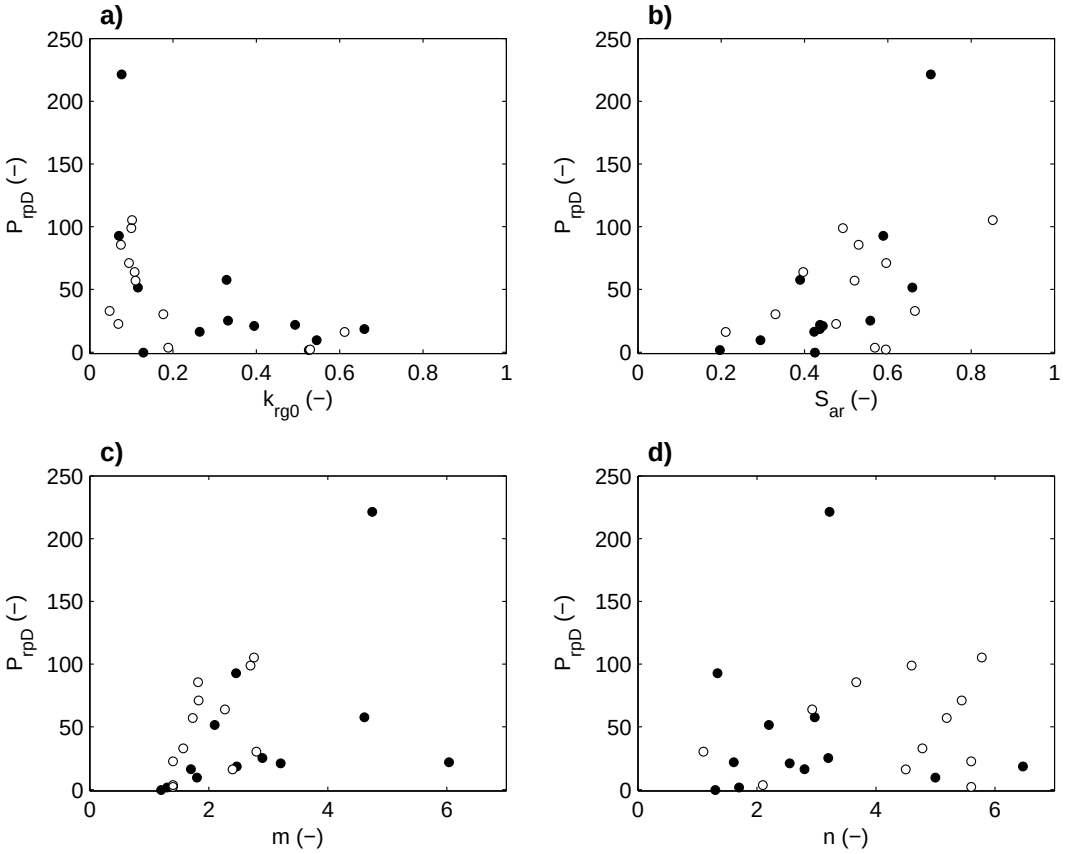

Figure 4: Plot of dimensionless pressure contribution due to relative permeability effects, P_{rpD}, against the four relative permeability parameters for all the relative permeability curves shown in Fig. 1. Closed and open circular markers represent the sandstone and carbonate cores, respectively.

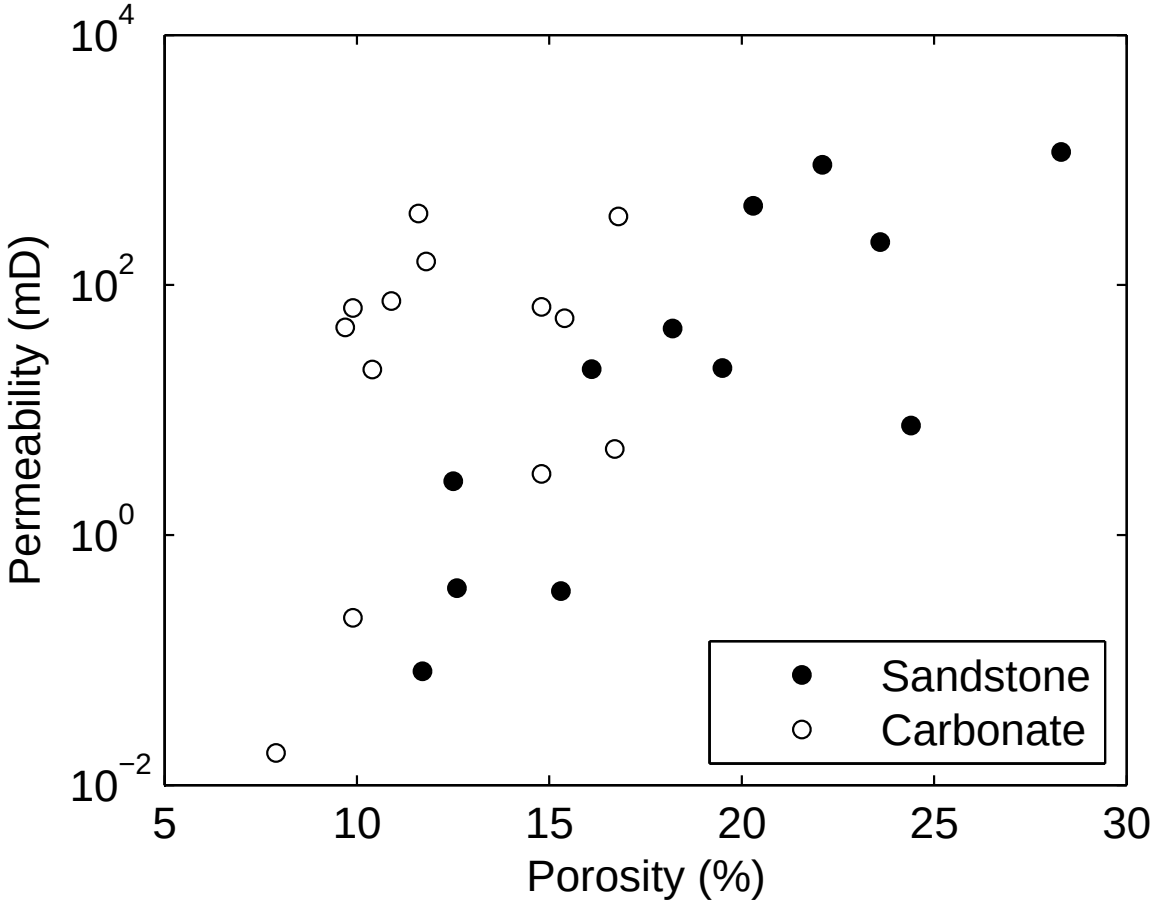

Figure 5: Plot of porosity against permeability for all the cores listed in Table 1. Closed and open circular markers represent the sandstone and carbonate cores, respectively.

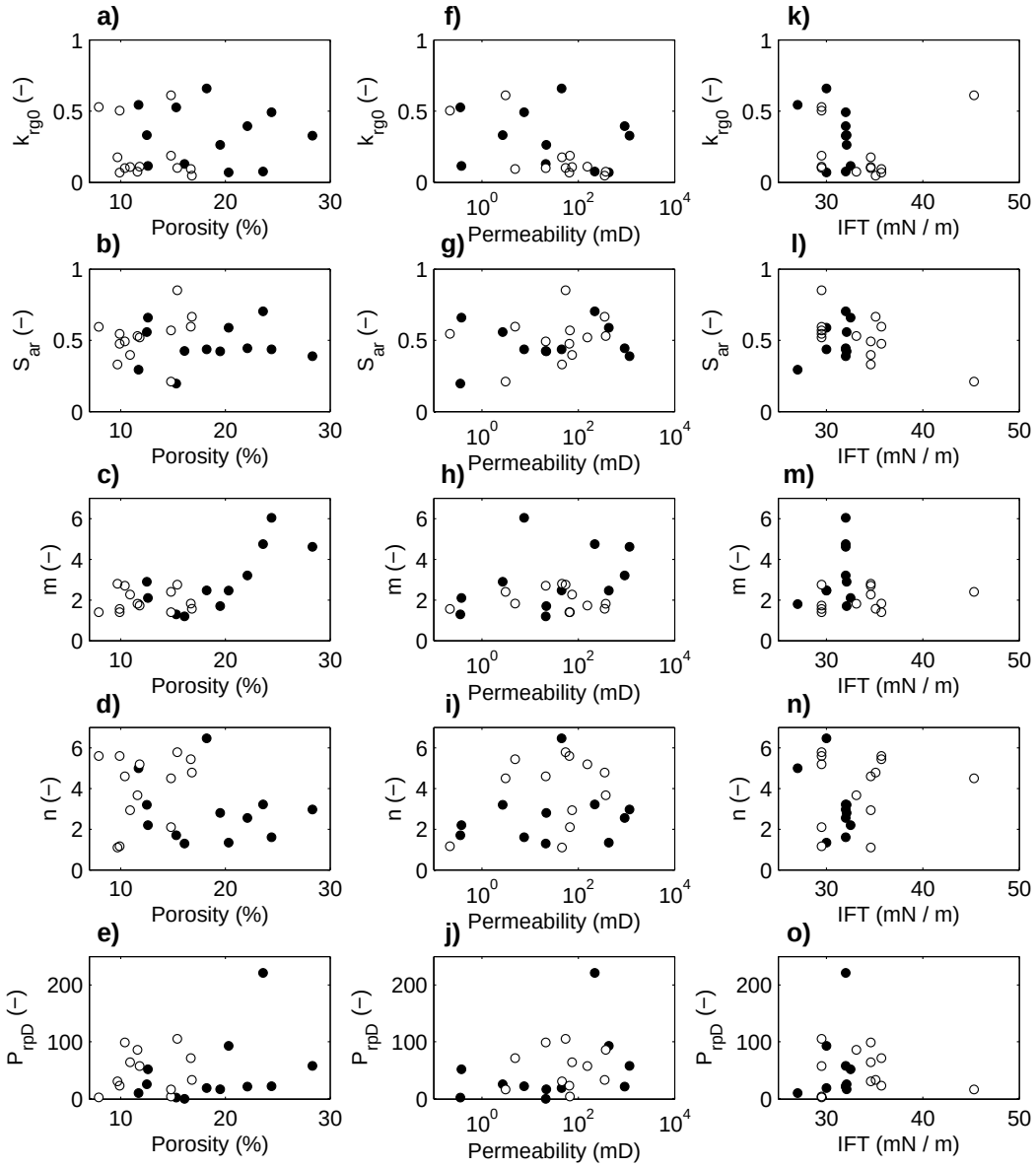

Figure 6: Plots of the four relative permeability parameters and dimensionless pressure contribution due to relative permeability effects, P_{rpD}, for all the cores listed in Table 1, against: a) to e) porosity, f) to j) permeability and k) to o) interfacial tension (IFT). Closed and open circular markers represent the sandstone and carbonate cores, respectively.

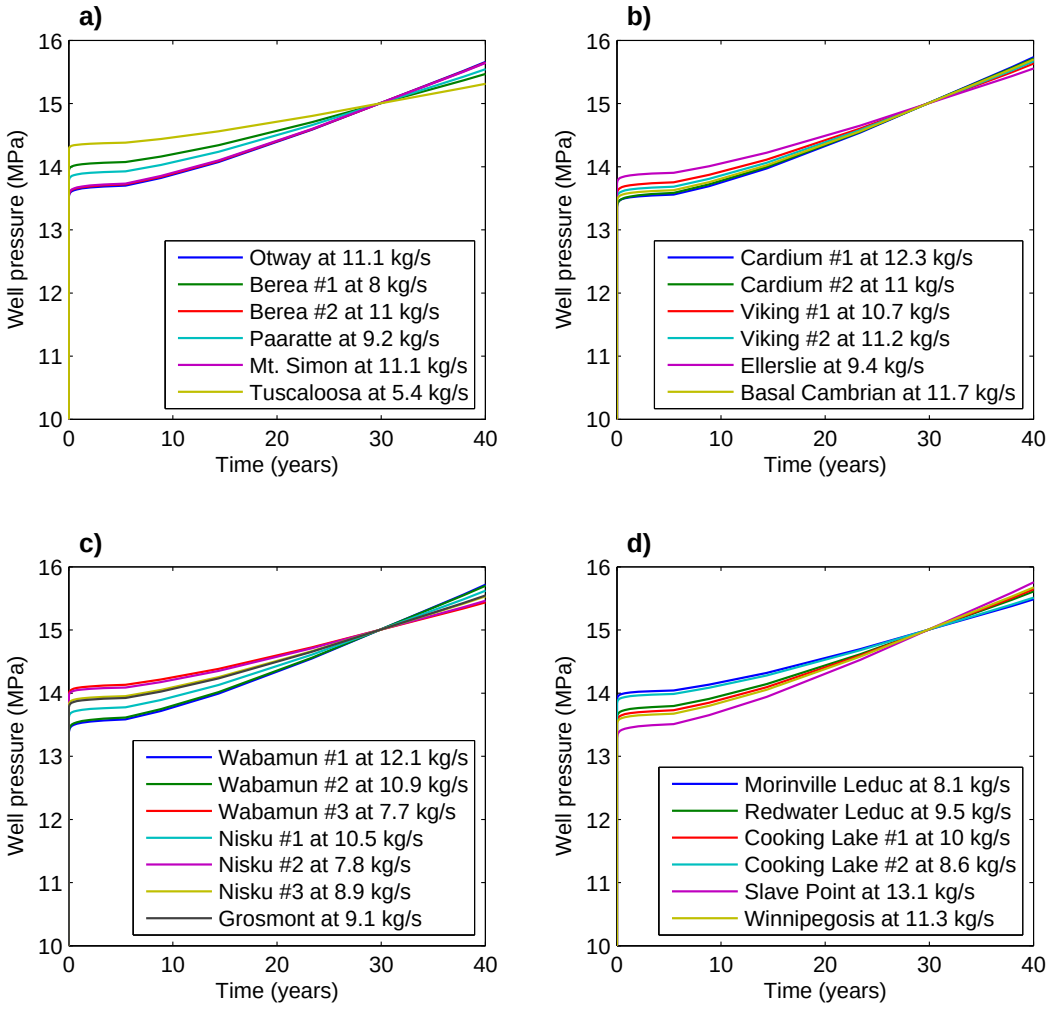

Figure 7: Comparison of simulated well pressures using the 25 different relative permeability parameter sets given in Table 1 and fixing the injection rate such that injection pressure equals 15 MPa after 30 years. See legend for injection rate values. See Table 3 for other parameters. a) Using relative permeability data from the sandstone cores of Perrin and Benson (2010) and Krevor et al. (2012). b) Using relative permeability data from the sandstone cores of Bennion and Bachu (2008). c) and d) Using relative permeability data from the carbonate cores of Bennion and Bachu (2010).

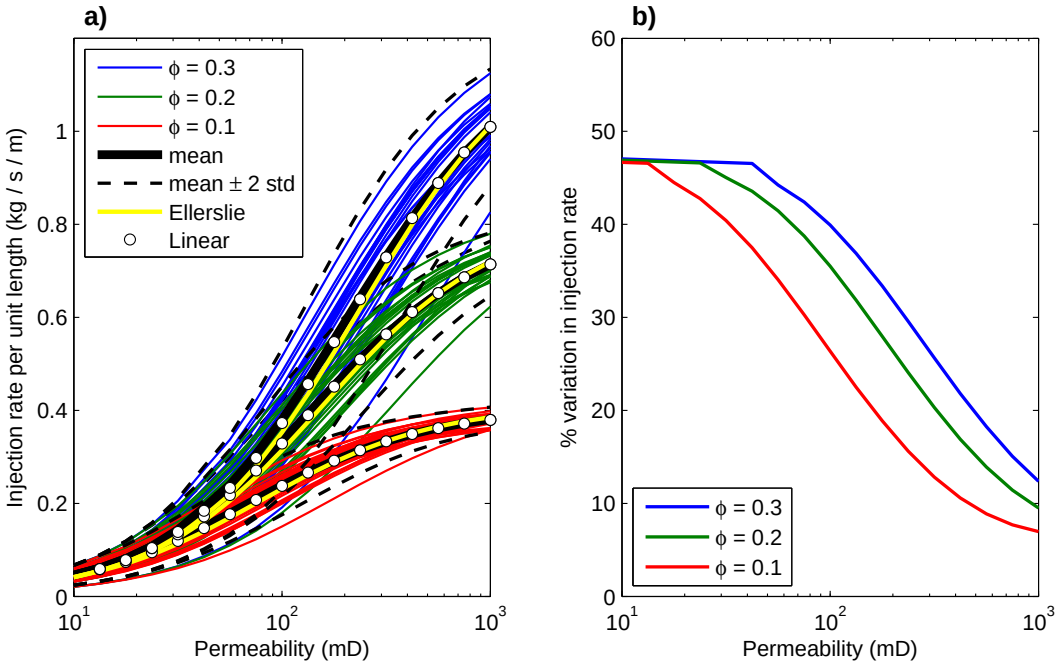

Figure 8: a) Plots of maximum sustainable injection rate per unit length (of fully completed vertical well bore) against permeability for different porosities. The thin solid lines are the results obtained for each of 25 relative permeability parameter sets (from Table 1) but assuming the porosities and permeabilities given by the lengend and x-axis, respectively. The black solid and dashed lines represent the mean and the mean ± two standard deviations (std) of the 25 relative permeability parameter sets (RPPS), respectively. The yellow solid line is due to the individual response of the Ellerslie sandstone RPPS. The white circular markers are results assuming linear relative permeability functions with $k_{rg0} = 0.1$ and $S_{ar} = 0.2$. b) Plots of percentage variation in injection rate (PVIR) (due to the range of responses derived from the 25 RPPS) against permeability for different porosities (obtained by dividing two standard deviations by the mean and multiplying by 100).

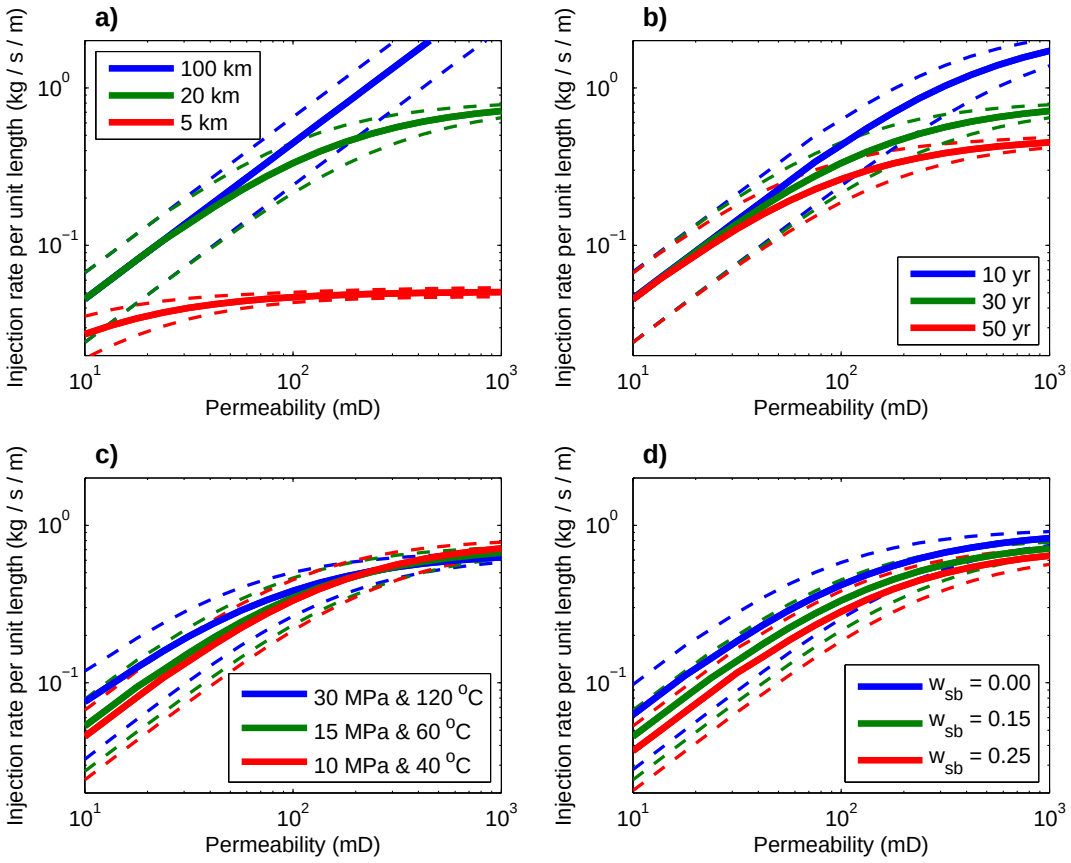

Figure 9: Similar to Fig. 8a but looking at: a) variation in radial extent of aquifer (r_E); b) variation in injection duration; c) variation in aquifer conditions; d) variation in formation water salt mass fraction (w_{sb}). The solid and dashed lines represent the mean and the mean ± two standard deviations (std) of the 25 RPPS, respectively.

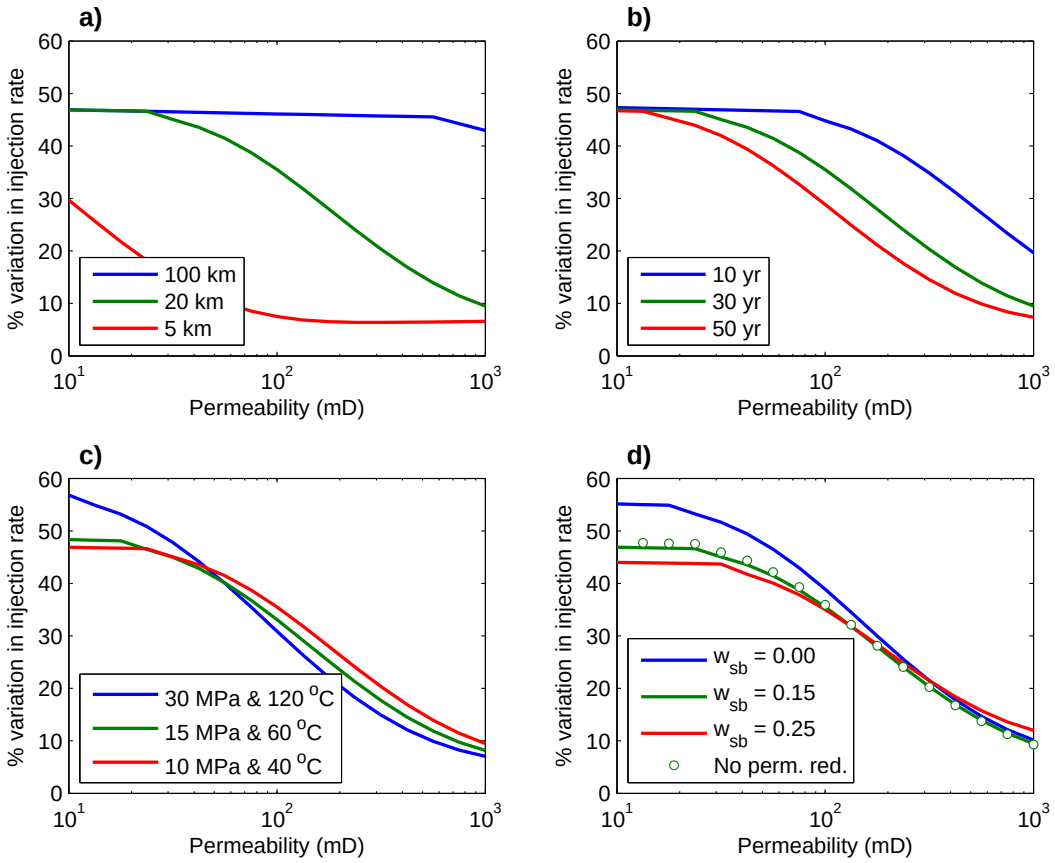

Figure 10: The same as Fig. 8b but looking at: a) variation in radial extent of aquifer (r_E); b) variation in injection duration; c) variation in reservoir conditions; d) variation in formation water salt mass fraction (w_{sb}).

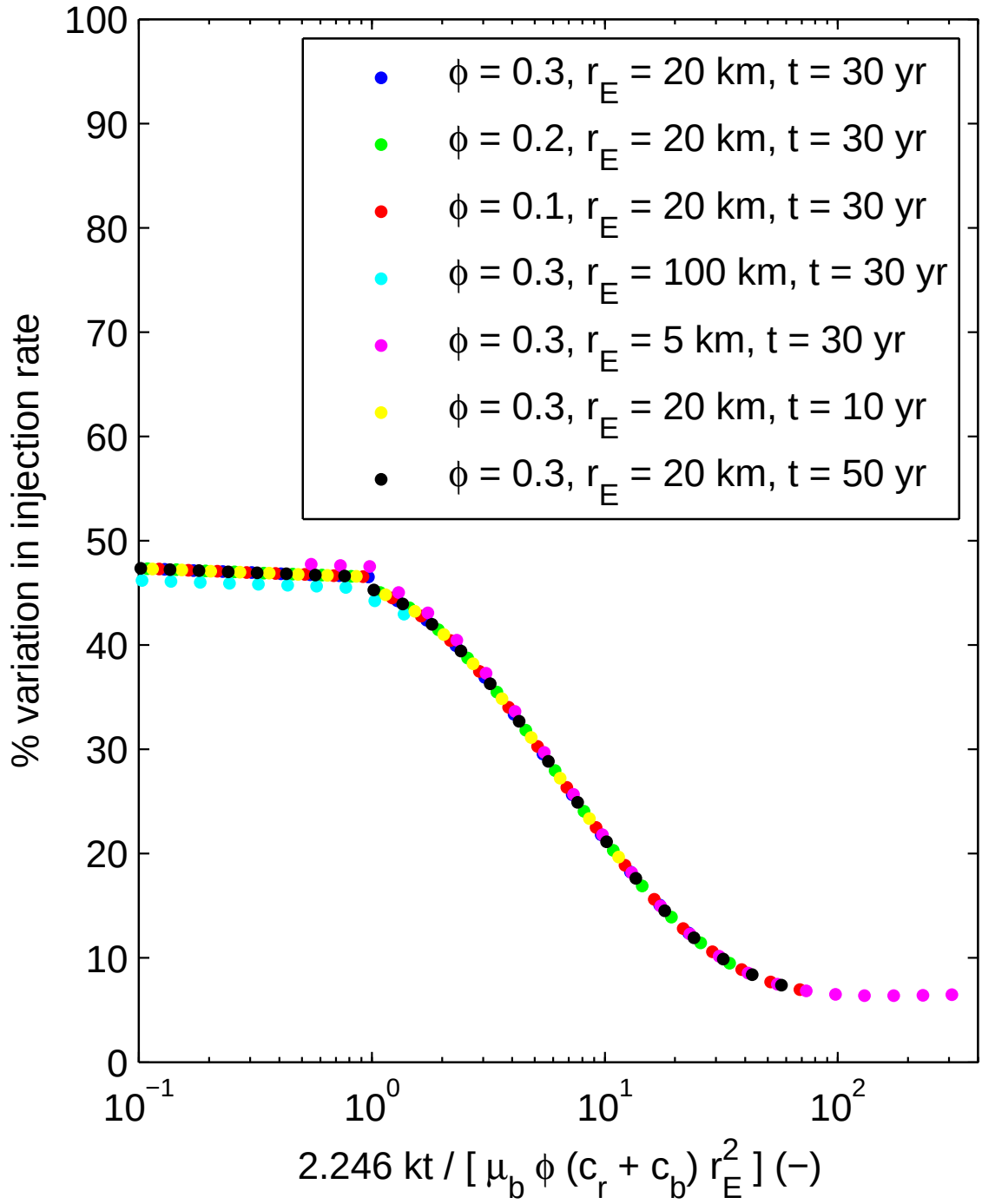

Figure 11: Plots of PVIR against dimensionless time, combining all the data previously presented in Figs. 8b, 10a and 10b.